Indian Journal of Pure & Applied Physics
Vol. 54, December 2016, pp.777-786

Conjugate heat and mass transfer in square porous cavity

Azeem[a,b], Irfan Anjum Badruddin[c]*, Mohd Yamani Idna Idris[a], N Nik-Ghazali[c], Salman Ahmed N J[d] & Abdullah A A A Al-Rashed[e]

[a]Department of Computer System & Technology, University of Malaya, Kuala Lumpur, Malaysia
[b]Department of Mathematics and Computer Science, Taylor's University, Kuala Lampur, Malaysia
[c]Department of Mechanical Engineering, University of Malaya, Kuala Lumpur, 50603, Malaysia
[d]Center for Energy Sciences, Department of Mechanical Engineering, University of Malaya, Kuala Lumpur, 50603, Malaysia
[e]Department of Automotive and Marine Engineering Technology, College of Technological Studies, The Public Authority for Applied Education and Training, Kuwait

Received 8 January 2016; revised 14 August 2016; accepted 29 August 2016

The present article deals with the issue of heat and mass transfer in a square porous cavity having a small solid wall or block inserted at various places at bottom surface. The main objective is to investigate the effect of size of solid wall and its location inside the porous cavity on double diffusive convention. The heat and mass transfer behavior are governed by momentum, energy and concentration equations which are converted into a set of finite element equation with the help of Galerkin method. The left surface of cavity is maintained at higher temperature and concentration, T_h and C_h as compared to that of right surface at T_c and C_c. The results are presented in terms of thermal, concentration and fluid flow profiles across the porous cavity.

Keywords: Porous cavity, Conjugate double diffusion, FEM

1 Introduction

The thorough understanding of the convective heat transfer and the fluid flow through porous medium have gained considerable attraction by the eminent researchers during the last few decades, as evident from the myriad number of articles published in this area. The deep insight to the fundamental concept of the heat transfer and fluid flow has been dealt meticulously by many authors, such as; Nield and Bejan[1], Ingham and Pop [2], Vafai[3], Pop and Ingham[4] and, Bejan and Kraus[5]. The conjugate heat transfer refers to a situation where heat transfer occurs simultaneously between fluid and solid emanating a complex boundary condition between fluid and solid, whereby it analyzes simultaneously heat transfer both in solid as well as fluid[6]. The different aspects of the convective heat transfer have been reported in the available literature[7-14], but conjugate heat transfer received relatively lesser attention. In conjugate heat transfer the solid fluid interface is governed by the conduction and convection phenomenon thus making it to more peculiar to analyze. Thus it becomes inevitable to solve the energy equations both in solid as well as fluid media simultaneously[15]. The ratio of the conductivity of the wall and the fluid and the wall thickness has profound effect on the heat transfer characteristics[16]. The effect of the wall heat conduction in an annulus region is also found to be significantly high as reported by the Shakibara *et al.*[17]. In a similar study, Tao[18] analyzed and reported that the ratio of the heat capacities of the fluids has significant effect on the finned tube heat transfer in a conjugate heat transfer analysis. Even though the conjugate heat transfer has received lesser attention in recent studies, however it is fairly understood that there has been considerable efforts made by many researchers to shed light on various aspects of the conjugate heat transfer as evident from the above literature. Apart from the conjugate heat transfer there has been growing interest on the effect of combined heat and mass transfer in both solid and fluid phase as it addresses many issues in the practical applications sought in the food processing industries. For instance Oliveira and Haghighi[19] have addressed the flow peculiarities to generate the temperature and the moisture contours during wood drying process. In another study similar attempt was made by Lamnatou *et al.*[20] for a square cylinder of a model food substrate where in emphasis was given on the flow blockage and its influence over heat and mass

*Corresponding author (E-mail: irfan_magami@rediffmail.com)

transfer. Thus few others also attempted to address the different aspects of the combined conjugate heat and mass transfer process in the literature[21-24]. The current work is aimed to understand the heat and fluid flow behavior due to presence of a solid wall/block inside the porous medium when its location is varied from left to right surface of cavity. The potential application of current problem can be found in grain storage rooms that have inbuilt platforms for sitting or other purposes.

2 Mathematical Model

The mathematical model of problem under investigation is based on momentum, energy and species concentration equations that are coupled together with suitable parameters. A square cavity filled with porous medium is considered with a small solid placed at various positions along the bottom surface as depicted in Fig. 1. The *x* and *y* coordinates are taken along horizontal and vertical directions, respectively. The left surface of cavity is maintained at temperature T_h and concentration C_c which are higher than its corresponding temperature and concentration at cold surface with notation T_c and C_c, respectively. The following assumptions are applied while investigation the heat and mass transfer behavior in porous cavity.

(i) The Darcy law is applicable in the porous medium.
(ii) The properties of the fluid and those of the porous medium are homogeneous.
(iii) Fluid properties are constant except the variation of density with temperature.
(iv) There is no phase change of fluid.

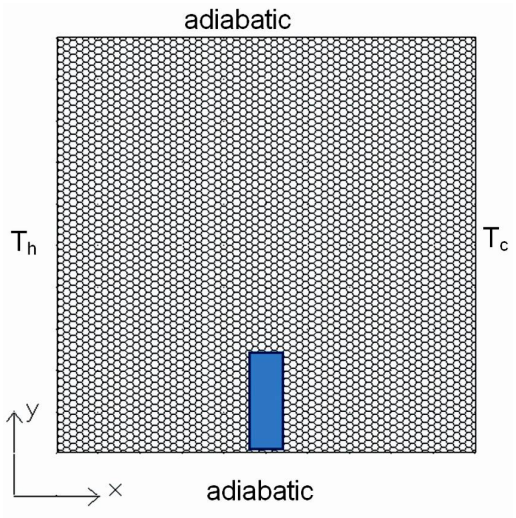

Fig. 1 ─ Porous cavity with solid

(v) The thermal equilibrium exists between fluid and solid phase of porous medium.

The governing equations resulting due to above mentioned problem are:

Continuity equation:

$$\frac{\partial u}{\partial x}+\frac{\partial \mathrm{v}}{\partial y}=0 \qquad \cdots (1)$$

Momentum equation:

$$\frac{\partial u}{\partial y}-\frac{\partial \mathrm{v}}{\partial x}=-\frac{g\beta K}{\nu}\frac{\partial T}{\partial x} \qquad \cdots (2)$$

Energy equation for porous medium:

$$u\frac{\partial T_p}{\partial x}+\mathrm{v}\frac{\partial T_p}{\partial y}=\alpha\left(\frac{\partial^2 T_p}{\partial x^2}+\frac{\partial^2 T_p}{\partial y^2}\right)-\frac{1}{\rho C_p}\frac{\partial q_r}{\partial x} \qquad \cdots (3)$$

Energy equation for solid:

$$\frac{\partial^2 T_s}{\partial x^2}+\frac{\partial^2 T_s}{\partial y^2}-\frac{1}{\alpha\rho C_p}\frac{\partial q_r}{\partial x}=0 \qquad \cdots (4)$$

Concentration equation:

$$u\frac{\partial C}{\partial x}+\mathrm{v}\frac{\partial C}{\partial y}=D\left(\frac{\partial^2 C}{\partial x^2}+\frac{\partial^2 C}{\partial y^2}\right) \qquad \cdots (5)$$

Subjected to boundary conditions:

at $x=0$ $u=0,\ v=0$ $T=T_h$ $C=C_h$ $\cdots$ (6a)

at $x=L$, $u=0,\ v=0$ $T=T_c$ $C=C_c$. $\cdots$ (6b)

at $y=0$ *and* $y=L$, $u=0,\ v=0$ $\frac{\partial T}{\partial y}=0$ $\cdots$ (6c)

The application of principal of no heat storage in the solid, results into following additional boundary conditions at solid porous interphase.

at $x=x_{sp}$ $u=0,\ v=0$ $T_s=T_p$

$$k_s\frac{\partial T_s}{\partial x}=k_p\frac{\partial T_p}{\partial x} \qquad \cdots (6d)$$

at $y=y_{sp}$ $u=0,\ v=0$

$$T_s=T_p\ k_s\frac{\partial T_s}{\partial y}=k_p\frac{\partial T_p}{\partial y} \qquad \cdots (6e)$$

Equation (1) can be satisfied automatically by introducing the stream function ψ as:

$$u=\frac{\partial \psi}{\partial y}\ \mathrm{v}=-\frac{\partial \psi}{\partial x} \qquad \cdots (7)$$

Following non-dimensional parameters are used:

$$\bar{x}=\frac{x}{L}\ ,\qquad \bar{y}=\frac{y}{L}\ ,\qquad \bar{\psi}=\frac{\psi}{\alpha}\ ,$$

$$\bar{T}=\frac{(T-T_c)}{(T_w-T_c)}\ ,\ \bar{C}=\frac{(C-C_c)}{(C_w-C_c)}$$

$$R_d = \frac{4\sigma T_c^{\,3}}{\beta_R k}\,,\; Ra = \frac{g\beta_T \Delta T K L_c}{\nu\alpha}\,,\qquad Le = \frac{\alpha}{D}\qquad,$$

$$N = \left(\frac{\beta_c \Delta C}{\beta_T \Delta T}\right)$$

Invoking Rossel and approximation for radiation:

$$q_r = -\frac{4\sigma}{3\beta_r}\frac{\partial T^4}{\partial x} \qquad \cdots (8)$$

Expanding T^4 in Taylor series about T_c and neglecting higher order terms [7,25-28]:

$$T^4 \approx 4TT_c^{\,3} - 3T_c^{\,4} \qquad \cdots (9)$$

Substituting Eqs (6-9) into Eqs (2-5) yields:

Momentum equation:

$$\frac{\partial^2 \overline{\psi}}{\partial \overline{x}^2} + \frac{\partial^2 \overline{\psi}}{\partial \overline{y}^2} = -Ra\left[\frac{\partial \overline{T}}{\partial \overline{x}} + N\frac{\partial \overline{C}}{\partial \overline{x}}\right] \qquad \cdots (10)$$

Energy equation of porous region:

$$\frac{\partial \overline{\psi}}{\partial \overline{y}}\frac{\partial \overline{T}}{\partial \overline{x}} - \frac{\partial \overline{\psi}}{\partial \overline{x}}\frac{\partial \overline{T}}{\partial \overline{y}} = \left(\left(1+\frac{4R_d}{3}\right)\frac{\partial^2 \overline{T}}{\partial \overline{x}^2} + \frac{\partial^2 \overline{T}}{\partial \overline{y}^2}\right) \qquad \cdots (11)$$

Energy equation in solid region:

$$\left(1+\frac{4R_d}{3}\right)\frac{\partial^2 \overline{T}}{\partial \overline{x}^2} + \frac{\partial^2 \overline{T}}{\partial \overline{y}^2} = 0 \qquad \cdots (12)$$

Concentration equation:

$$\frac{\partial \overline{\psi}}{\partial \overline{y}}\frac{\partial \overline{C}}{\partial \overline{x}} - \frac{\partial \overline{\psi}}{\partial \overline{x}}\frac{\partial \overline{C}}{\partial \overline{y}} = \frac{1}{Le}\left(\frac{\partial^2 \overline{C}}{\partial \overline{x}^2} + \frac{\partial^2 \overline{C}}{\partial \overline{y}^2}\right) \qquad \cdots (13)$$

The corresponding boundary conditions are:

At $\overline{x} = 0 \quad \overline{\psi} = 0 \quad \overline{T} = 1 \quad \overline{C} = 1$ … (14a)

At $\overline{x} = 1 \quad \overline{\psi} = 0 \quad \overline{T} = 0 \quad \overline{C} = 0$ … (14b)

At $\overline{y} = 0 \quad and \quad \overline{y} = 1,\ \overline{\psi} = 0 \quad \dfrac{\partial \overline{T}}{\partial \overline{y}} = 0$ … (14c)

At $\overline{x} = x_{sp} \quad \overline{\psi} = 0,\ Kr\dfrac{\partial \overline{T}_s}{\partial \overline{x}} = \dfrac{\partial \overline{T}_p}{\partial \overline{x}}$ … (14d)

At $\overline{y} = \overline{y}_{sp} \quad \overline{\psi} = 0 \quad Kr\dfrac{\partial \overline{T}_s}{\partial \overline{y}} = \dfrac{\partial \overline{T}_p}{\partial \overline{y}}$ … (14e)

The heat and mass transfer rate at the hot surface can be calculated using following relations:

$$Nu = -\left(\left(1+\frac{4}{3}R_d\right)\frac{\partial \overline{T}}{\partial \overline{x}}\right)_{\overline{x}=0} \qquad \cdots (15)$$

The Sherwood number is expressed as:

$$Sh = \left(-\frac{\partial \overline{C}}{\partial \overline{x}}\right)_{\overline{x}=0} \qquad \cdots (16)$$

3 Numerical Scheme

It is worth mentioning that the present problem is governed by 4 partial differential Eqs (10-13) subjected to complex boundary conditions as given in Eq. 14. These set of equations are difficult to solve directly. Therefore as an alternate solution technique, finite element method is used to arrive at solution. The above mentioned equations are converted into matrix form of equations with the help of Galerkin method. Total of 2592 triangular elements are used to divide the physical domain into smaller segments. An iterative algorithm is adopted to solve the resulting finite element equations. The convergence criteria for $\overline{\psi}$, $\overline{T}$ and $\overline{C}$ are set at 10^{-7}, 10^{-5} and 10^{-5}, respectively. The accuracy of current method is verified by comparing the results with data available in open literature. In order to compare the results, the solid wall/block thickness and height was reduced to zero along with buoyancy ratio and Lewis number set at 0 and 1 respectively so that it corresponds to the case of available data. It is clear from Table 1 that the present method is accurate enough for the case under investigation.

4 Results and Discussion

4.1 Temperature, concentration and fluid profile

The following section describes the results obtained for various geometrical as well as physical parameters that affect the conjugate heat and mass transfer in a square porous cavity. Figure 2 represents the heat and mass transfer behavior in terms of isotherms, iso-concentration lines and streamlines reflecting the temperature, concentration and velocity distribution in the square cavity. This figure is

Table 1 ─ Validation of results

Author	$Ra = 10$	$Ra = 100$
Present	1.0821	3.2126
Walker and Homsy[29]		3.097
Bejan[30]		4.2
Gross *et al.*[31]		3.141
Monolo & Lage[32]		3.118
Beckerman *et al.*[33]		3.113
Moya *et al.*[34]	1.065	2.801
Baytas & Pop[35]	1.079	3.16
Misirlioglu *et al.*[36]	1.119	3.05

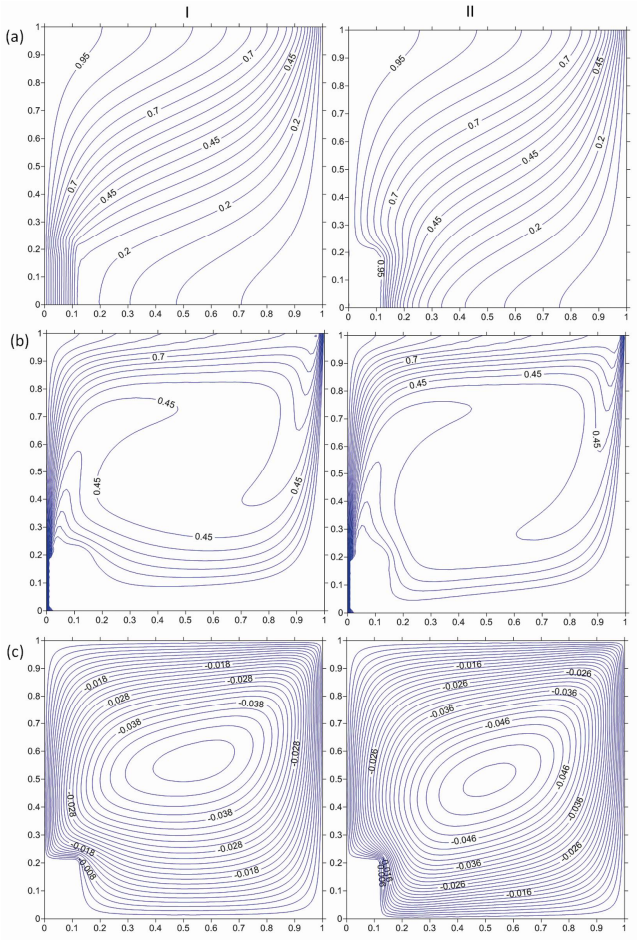

Fig. 2 — Effect of *Kr* and solid (S_h=*0.2*) at $\bar{x} = 0$, (I) *Kr* = 0.1 (II) *Kr=25*; (a) Isotherms (b) Iso-concentration and (c) Streamlines

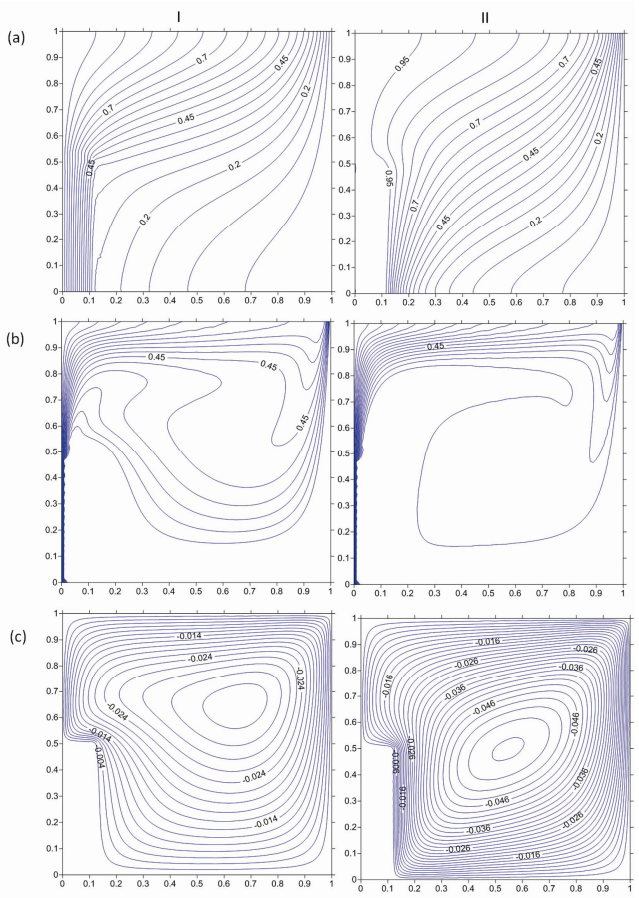

Fig. 3 — Effect of *Kr* and solid (S_h=*0.5*) at $\bar{x} = 0$, (I) *Kr* = 0.1 (II) *Kr=25*; (a) Isotherms (b) Iso-concentration and (c) Streamlines

obtained by setting the parameters as $Ra = 100, Rd = 0.5, N = 0.2, L = 10$, for solid wall placed at the left surface of cavity with S_h=0.2. The geometric parameter S_h is ratio of height of solid wall to the height of porous cavity thus S_h=*0.2* indicates that the height of solid wall is 20% of total cavity height. The left column of Fig. 2 corresponds to *Kr=0.1* whereas the right column belongs to *Kr=25*.

Based on the results presented in Fig. 2, it is obvious that the isotherms penetrate deeper into the porous medium due to increased conductivity ratio, *Kr*. It should be noted that the conductivity ratio *Kr* represents the thermal conductivity ratio of solid wall to the porous medium. A value of *Kr*>1 indicates that the solid wall conductivity is higher than that of porous medium and vice versa for *Kr<1*. It can be conveniently said that the larger area of cavity is occupied with high concentration lines for *Kr=0.1* than that of *Kr*=25 as reflected by Fig. 2. This can be inferred from iso-concentration lines where more than 50% of porous region is occupied by $\bar{C} \geq 0.45$ at *Kr=0.1* than that of *Kr*=25. This could be the result of higher fluid velocity at smaller value of *Kr* as illustrated by streamlines of Fig. 2 where magnitude of stream-function is higher at *Kr=0.1* than that of *Kr=25*. The effect of solid placed at left wall of cavity is further investigated (Fig. 3) when height of solid wall is increased from 20% (S_h=*0.2*) to 50% (S_h=*0.5*) keeping all other parameters same as corresponding to that of Fig. 2. The convective heat transfer rate at top of cavity increases due to increased thermal gradient in that area for S_h=*0.5* as compared to S_h=*0.2*. The high concentration area reduces owing to increase in solid height. The effect of solid wall is much more pronounced at *Kr=0.1* than that of *Kr=25*. This is a result of fluid cell which changes flow pattern from being oval to near circular. Furthermore, the fluid movement shifts the whole of the cell in upward section of cavity at *Kr=0.1*. This combined effect of fluid cell affects the concentration distribution to a greater extent. The aim of present work is to study the

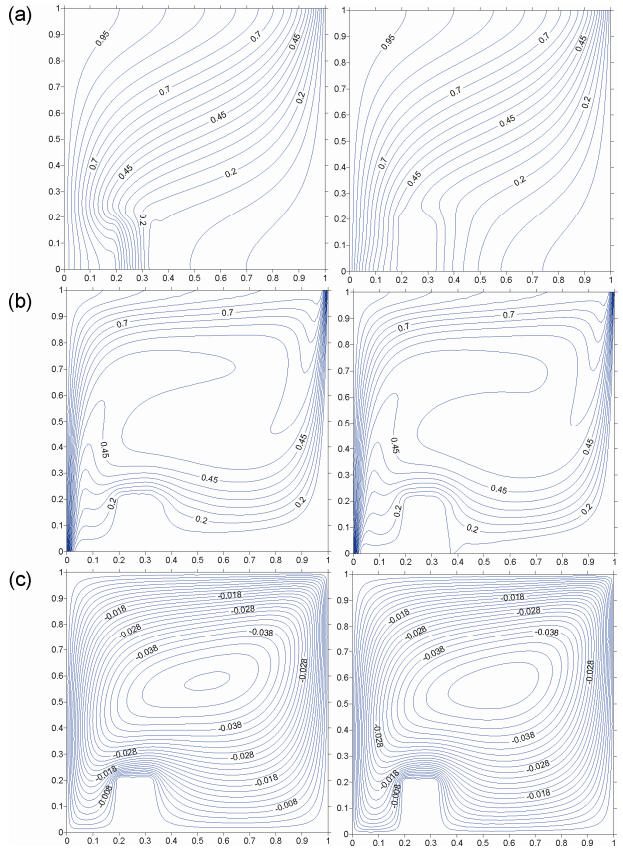

Fig. 4 — Effect of *Kr* and solid (S_h=*0.2*) at $\bar{x} = 0.25L$, (I) *Kr* = 0.1 (II) *Kr=25*; (a) Isotherms (b) Iso-concentration and (c) Streamlines

size as well as location of solid wall in the porous medium. In this regard, the location of solid is varied at 5 places such as at $\bar{x} = 0$,$\bar{x} = 0.25L$, $\bar{x} = 0.5L$, $\bar{x} = 0.75L$ and $\bar{x} = L$. Figures 2 and 3 corresponded to $\bar{x} = 0$ whereas Fig. 4 shows the heat and mass transfer behavior when solid is placed at $\bar{x} = 0.25L$. Other parameters for Fig. 3 are set at $a = 100, Rd = 0.5, N = 0.2, L = 10$. It is observed that the heat transfer rate from hot wall to porous medium does not change much at *Kr=0.1* from its counterpart of solid being placed at left wall ($\bar{x} = 0, \text{Fig. } 2$). However, there is an important observation that needs to be elaborated that the temperature variation inside the solid wall decreases owing to change of solid wall location. The temperature variation in solid wall further decreases at higher *Kr* as shown by isotherms of Figs 2-4, corresponding to *Kr=25*. This behavior can be attributed to the fact that the thermal conductivity and temperature difference in a solid are inversely related to each other, thus the increased *Kr* is an indication of higher thermal conductivity of solid wall which in turn helps in reducing the temperature difference across the solid. The

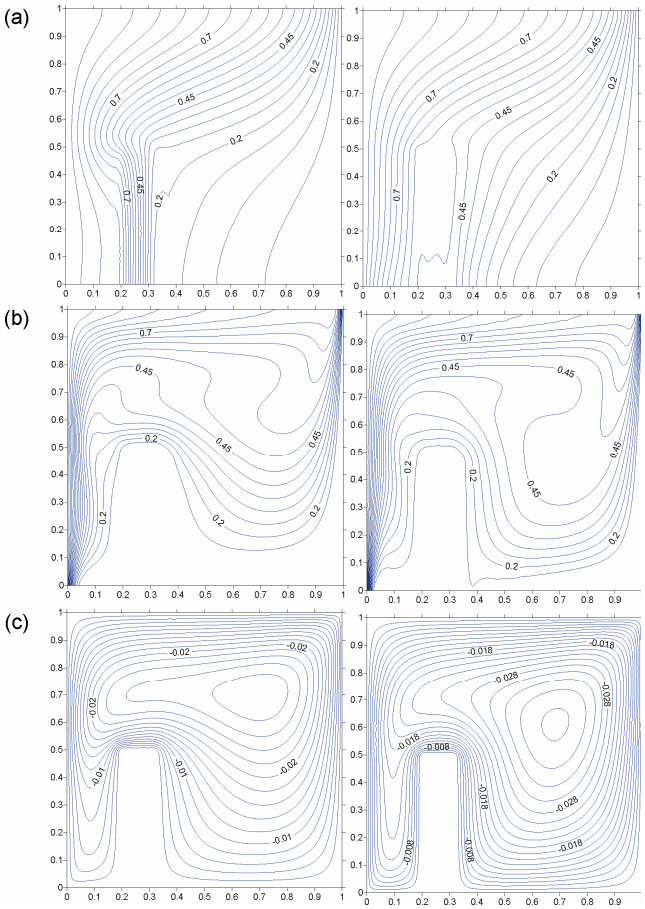

Fig. 5 — Effect of *Kr* and solid (S_h=*0.5*) at $\bar{x} = 0.25L$, (I) *Kr* = 0.1 (II) *Kr=25*; (a) Isotherms (b) Iso-concentration and (c) Streamlines

concentration diffusion seems to re-arrange itself due to presence of an obstruction in the form of solid wall. The increased solid height reduces the heat content of porous medium to the right of solid wall as shown in Fig. 5. It is noticeable that the temperature variation across solid wall increases at *Kr=0.1* when the height of solid is increased to 50%. The concentration distribution shifts towards upward section of cavity due to increased obstruction. However, this obstruction is overcome by some extent, due to increased fluid velocity for the case of *Kr=25*, thus filling the lower section of cavity with low concentration lines. The placement of solid wall at center of cavity, i.e., $\bar{x} = 0.5L$, further reduces the temperature difference across the solid as follows from Fig. 6. This is because of the reason that the availability of thermal energy decreases as one move from hot to cold surface of porous cavity which is indicated in Figs 2 and 4. Thus leading to decrease in temperature variation inside the solid wall placed far away from hot surface.The concentration profiles

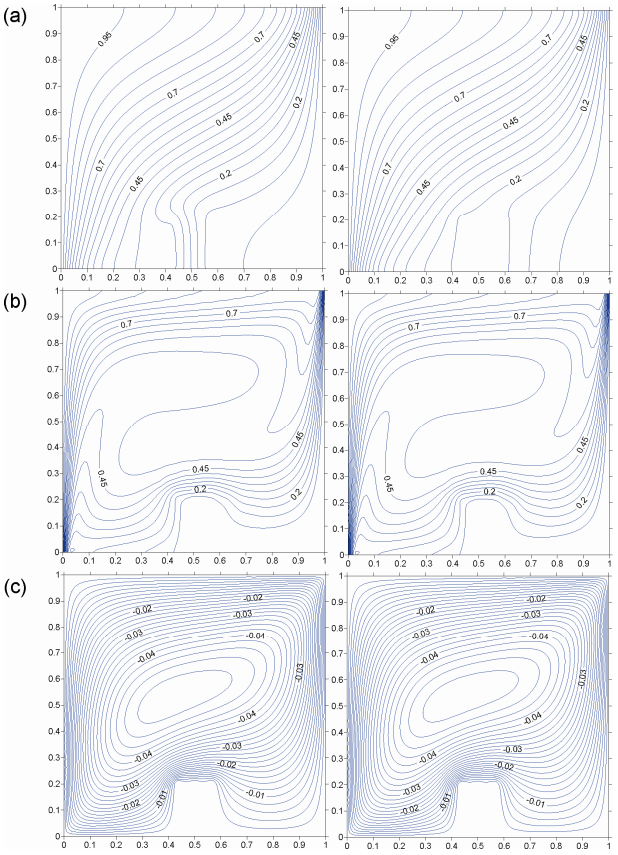

Fig. 6 — Effect of *Kr* and solid (S_h=*0.2*) at $\bar{x} = 0.5L$, (I) *Kr* = 0.1 (II) *Kr=25*; (a) Isotherms (b) Iso-concentration and (c) Streamlines

moves little bit upward direction as compared to Figs 2 and 4 with similar solid height. The fluid flow has distinct pattern as compared to other cases (Figs 2-6) when solid with S_h=*0.5* is placed at centerof cavity. The flow pattern is very close to splitting the fluid into two cells at *Kr=25* as outlined in Fig. 7. The temperature in the solid further declines as shown in Fig. 8 when the solid is moved to $\bar{x} = 0.75L$, as compared to the cases discussed earlier in this paper. This is clear indication of inability of heat to reach far away region of porous cavity towards the cold surface. However, it is noted that the effect of thermal conductivity ratio on concentration profile as well as fluid profile diminishes for solid (S_h=*0.2*) placed at $\bar{x} = 0.75L$. However, the increased solid height (S_h=*0.5)* at this location brings in little bit variation of concentration and fluid profile with respect to variation in *Kr* as demonstrated by Fig. 9. It is noted that the heat content of solid wall is minimum when it is placed at right surface of cavity as shown in Fig. 10 as compared to all other cases. Only two isotherms are affected by presence of solid wall at *Kr=0.1*. However, the increase in solid height to 50%

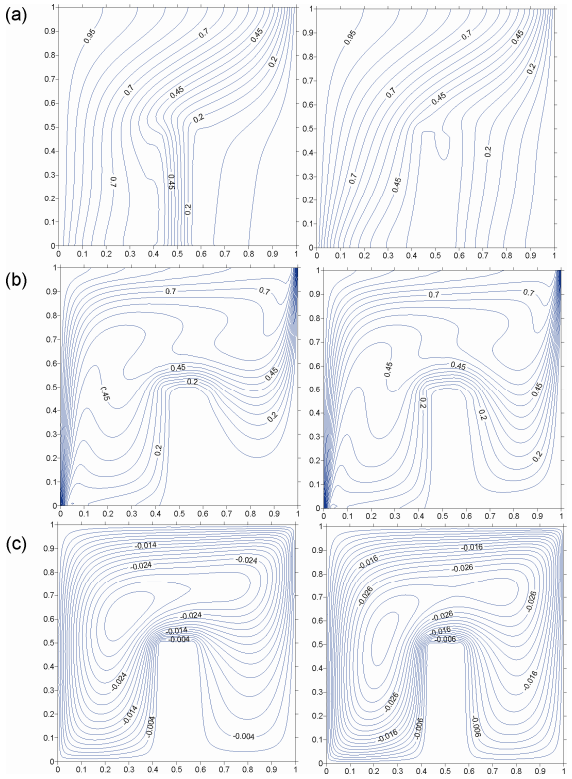

Fig. 7 — Effect of *Kr* and solid (S_h=*0.5*) at $\bar{x} = 0.25L$, (I) *Kr* = 0.1 (II) *Kr=25*; (a) Isotherms (b) Iso-concentration and (c) Streamlines

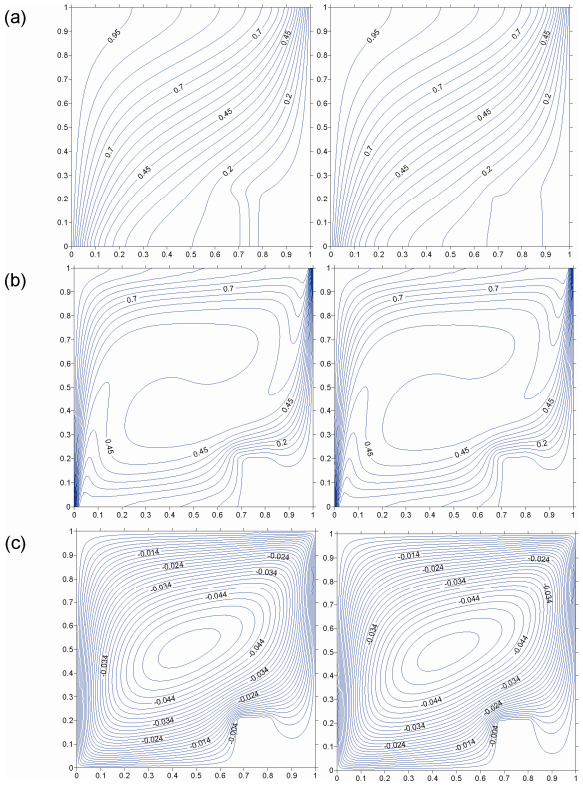

Fig. 8 — Effect of *Kr* and solid (S_h=*0.2*) at $\bar{x} = 0.75L$, (I) *Kr* = 0.1 (II) *Kr=25*; (a) Isotherms (b) Iso-concentration and (c) Streamlines

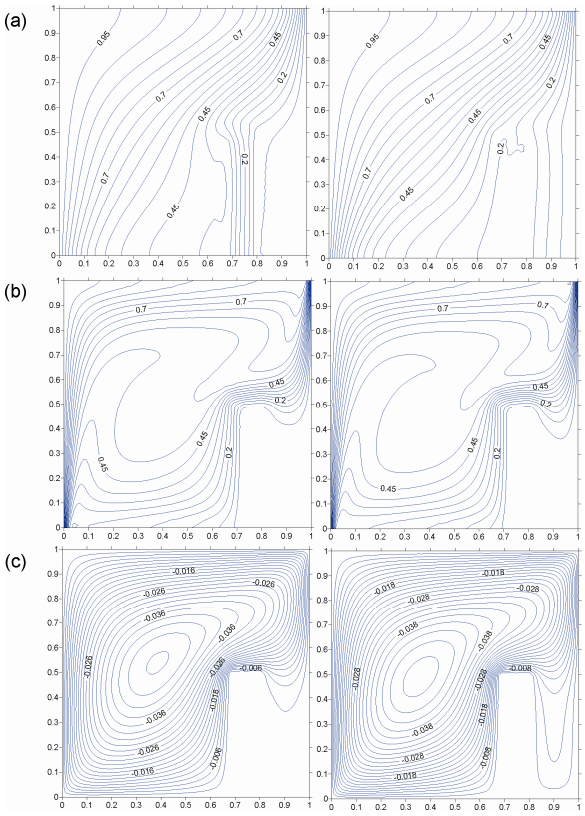

Fig. 9 — Effect of *Kr* and solid (S_h=*0.5*) at $\bar{x} = 0.25L$, (I) *Kr* = 0.1 (II) *Kr=25*; (a) Isotherms (b) Iso-concentration and (c) Streamlines

improves the heat content of solid as depicted in Fig. 11. The concentration and streamlines are not much affected with respect to *Kr* when solid wall is placed at right surface. The magnitude of stream function is found to be maximum when the solid wall is placed at right surface (Figs 10 and 11).

4.2 Heat and mass transfer

The following section presents the details of heat and mass transfer in terms of Nusselt and Sherwood number at hot surface of the cavity. The variation of Nusselt and Sherwood number along the hot wall as well as with height and location of solid are illustrated in Figs 12 and 13 and Table 2. The other parameters for these figures and table are kept as $Ra = 100, Rd = 0.5$. It should be noted that the Nusselt and Sherwood number is represented by temperature and concentration gradients at hot surface as given by Eqs 15 and 16, respectively. It is noted that the local Nusselt and Sherwood number generally decreases along the height of cavity (figure not shown to conserve the space). However, the variation follows different trend when solid is placed at $\bar{x} = 0.25$ as shown in Figs 12 and 13. In this case, the Nusselt number decreases slightly at bottom of cavity and the

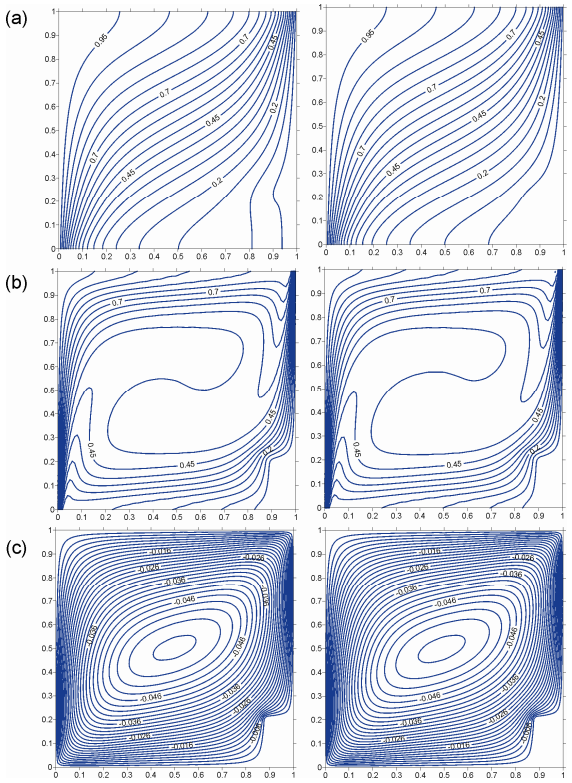

Fig. 10 — Effect of *Kr* and solid (S_h=*0.2*) at $\bar{x} = L$, (I) *Kr* = 0.1 (II) *Kr=25*; (a) Isotherms (b) Iso-concentration and (c) Streamlines

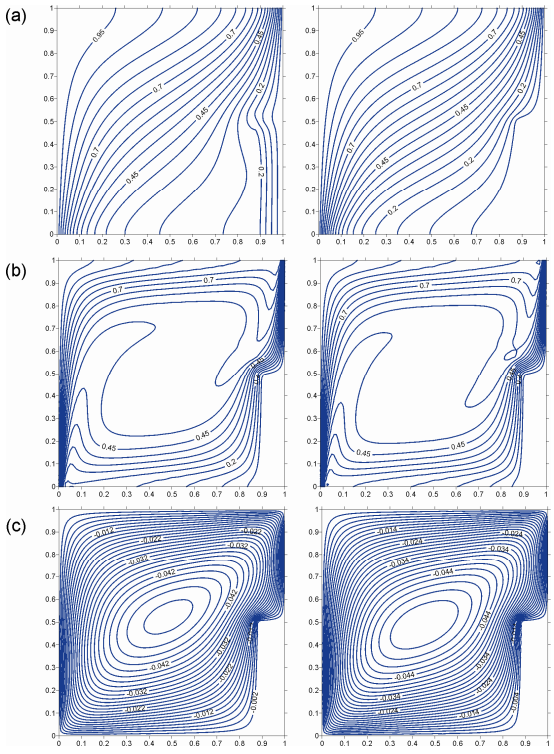

Fig. 11 — Effect of *Kr* and solid (S_h=*0.5*) at $\bar{x} = L$, (I) *Kr* = 0.1 (II) *Kr=25*; (a) Isotherms (b) Iso-concentration and (c) Streamlines

increases until a point thereafter it starts declining again when porous conductivity is much higher than that of solid wall conductivity (*Kr=0.1*). This could be best argued in a way that the presence of a low thermal conductivity solid increases the thermal resistance for heat to flow into porous medium through solid wall thus forcing the heat to find an alternate path of flow. This alternate path exists above the solid wall thus the heat transfer rate increases until the solid height and thereafter it declines due to fluid movement towards the cold surface. However, this behavior of increasing Nusselt number until solid height is suppressed when the conductivity of solid increases *(Kr=5)*. In this case, the thermal energy is easily transferred across the solid wall thus not forcing it to find an alternate path. The Nusselt number decreases continuously along the height of cavity though in a bilinear pattern. The Sherwood number decreases continuously except for the case of *Kr=0.1* and S_h*=0.5*, where it increases slightly at middle of the hot surface. This could be attributed to increased fluid movement just around the top corner of solid wall which helps in higher mass diffusion as depicted by streamlines of Fig. 5. It is found that the Nusselt number for the smaller value of conductivity ratio (*Kr=0.1*) decreases in a non-linear pattern along the height of cavity. This is very much compatible with the previous studies being carried out for the case of heat transfer in porous cavity [27]. The average Nusselt number decreases with increase in thermal conductivity ratio and height of solid block. It can be said that the higher thermal conductivity ratio creates low thermal gradient just above the solid due to higher thermal diffusion assisted by increased thermal

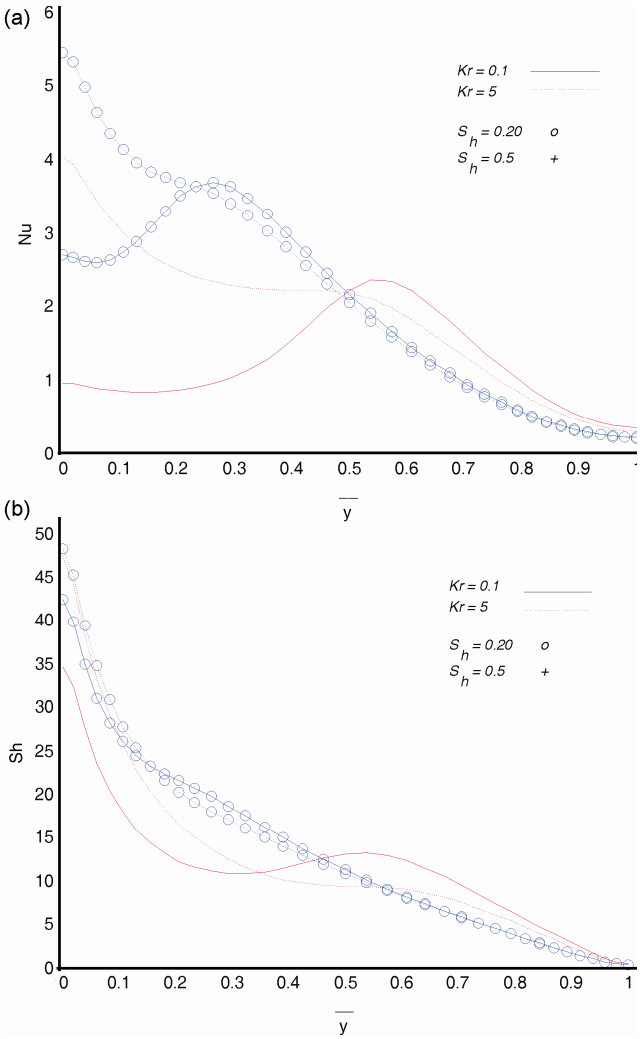

Fig. 12 — Nusselt number for solid $\bar{x}$ = 0.25L

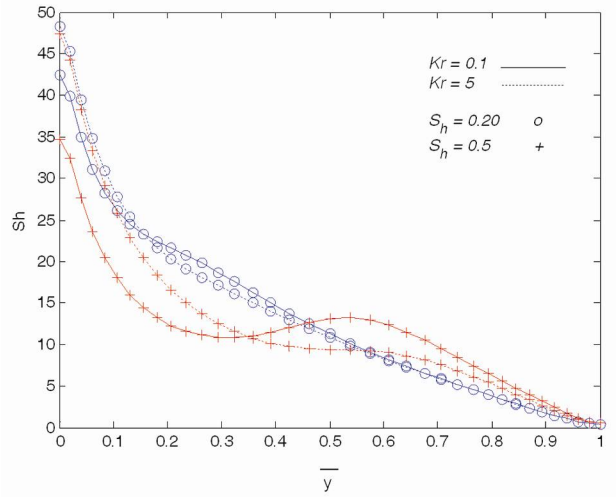

Fig. 13 — Sherwood number for solid at $\bar{x}$ = 0.25L

Table 2 — Average Nusselt and Sherwood number due to various location of block

Location of solid	Kr = 0.1, S_h = 0.2		Kr = 0.1, S_h = 0.5		Kr = 5, S_h = 0.2		Kr = 5, S_h = 0.5	
	$\overline{Nu}$	$\overline{Sh}$	$\overline{Nu}$	$\overline{Sh}$	$\overline{Nu}$	$\overline{Sh}$	$\overline{Nu}$	$\overline{Sh}$
$\bar{x}$ = 0	2.16110	12.6884	1.79968	13.5563	1.25536	13.1338	0.61740	13.7104
$\bar{x}$ = 0.25	1.89673	13.9337	1.14405	11.7251	2.26030	14.2373	1.88517	13.2128
$\bar{x}$ = 0.5	2.20771	13.6351	1.23749	11.9339	2.37668	13.7554	1.76102	13.0641
x □ = 0.75	2.39759	13.5526	1.59407	11.9729	2.50917	13.6097	2.05004	12.4236
$\bar{x}$ = 1	2.53201	13.6263	2.01892	12.6433	2.65048	13.6571	2.59887	12.9924

conductivity of solid. This is further vindicated by a curved isotherm near the hot wall when *Kr* is higher as compared to almost straight isotherm when *Kr* =0.1 of Figs 2 and 3. Similar trend of Nusselt number is seen when height of solid is increased from 20% to 50%. The Sherwood number also decreases with increase in height of cavity as depicted in Fig. 13.

5 Conclusions

The aim of present article was to investigate the effect of thermal conductivity ratio and placement of a solid in the square porous cavity. The investigation was carried out with respect to heat and mass transfer. Finite element method was used to solve the governing equations. The study revealed that the placement of solid has significant effect on the heat and mass transfer behavior in the cavity. It is found that the larger area of cavity is occupied by high concentration lines at low value of thermal conductivity ratio. It is further noted that the temperature variation inside the solid wall decreases owing to shifting of solid wall towards the right surface. The increased solid height moves the concentration distribution towards upward section of cavity. The stream function value is maximum for the case of solid wall placed at right surface of cavity. The Nusselt number is much affected due to solid location as compared to Sherwood number. The variation in Nusselt and Sherwood number follows multilinear pattern when solid is placed near the hot surface but this effect diminished when the placement of solid is moved towards the cold surface. The influence of thermal conductivity is stronger for longer solid as compared to its shorter version.

Nomenclature

C_p	Specific heat of fluid (J/kg-^{o}C)
$C, \overline{C}$	Species concentration
g	Acceleration due to gravity (m/s^2)
k	Thermal conductivity (W/m-^{o}C)
k_p ,k_s	Porous and solid thermal conductivity respectively (W/m-^{o}C)
K	Permeability of porous medium (m^2)
Kr	Conductivity ratio
L	Height and length of cavity (m)
Le	Lewis number
Nu	*N*usselt number
N	Buoyancy ratio
q_r	Radiation flux (W/m^2)
R_d	Radiation parameter
Ra	Modified Raleigh number
Sh	Sherwood number
S_h	Solid height
$T, \overline{T}$	Temperature
u, v	Velocity components in x and y direction respectively (m/s)
x, y	Cartesian co-ordinates
$\overline{x}, \overline{y}$	Non-dimensional co-ordinates

Greek Symbols

α	Thermal diffusivity (m^2/s)
β	Coefficient of thermal expansion (1/°C)
ρ	Density (kg/m^3)
ν	Coefficient of kinematic viscosity(m^2/s)
σ	Stephan Boltzmann constant (W/m^2-K^4)
β_r	Absorption coefficient (1/m)
ψ	Stream function
$\overline{\psi}$	Non-dimensional stream function

Subscripts

h	Hot
c	Cold
p	Porous
s	Solid

References

1 Nield D & Bejan A, *Convection in porous media*, Ed 3rd New (York: Springer Verlag), 2006.

2 Ingham D B & Pop I (Eds), *Transport phenomena in porous media*, (Pergamon: Oxford), 1998.

3 Vafai K, *Hand book of porous media*, (Marcel Dekker: New York), 2000.

4 Pop I & Ingham D B, *Convective heat transfer: Mathematical and computational modeling of viscous fluids and porous media*, (Pergamon: Oxford), 2001.

5 Bejan A D & Kraus, *Heat transfer handbook*, (Wiley: New York), 2003.

6 Joshi Y & Nakayama W, *Forced convection: external flows*, Edited by: Bejan A, Kraus A D, *Heat Transfer Handbook*, (John Wiley & Sons: Hoboken), 2003.

7 Raptis A, *Int Commun Heat Mass Trans*, 25 (1998) 289.

8 Ogulu A & Amos E, *Int Commun Heat Mass Trans*, 32 (2005) 974.

9 Kumaran V & Pop I, *Int J Heat Mass Trans*, 49 (2006) 3240.

10 Ahmed N J S, Badruddin I A, Zainal Z A, Khaleed H M T & Kanesan J, *Int J Heat Mass Trans*, 52 (2009) 3070.

11 Ahmed N J S, Badruddin I A, Kanesan J, Zainal Z A & Ahamed K S N, *Int J Heat Mass Trans*, 54 (2011) 3822.

12 Badruddin I A, Abdullah A A A A, Ahmed N J S & Kamangar S, *Int J Heat Mass Trans*, 55 (2012) 2184.

13 Badruddin I A, Ahmed N J S, Al-Rashed A A A A, Kanesan J, Kamangar S & Khaleed H M T, *Transport Porous Med*, 91(2) (2012) 697.

14 Badruddin I A, Al-Rashed A A A A, Ahmed N J S, Kamangar S & Jeevan K, *Int J Heat Mass Trans*, 55 (2012) 7175.

15 Iqbal Z, Syed K S & Ishaq M, *Int J Therm Sci*, 94 (2015) 242.

16 Mori S, Sakakibara M & Tanimoto A, *Heat Trans-Jpn Res*, 3 (1974) 37.

17 Mikio S, Shigeru M & Tanimoto A, *Can J Chem Eng*, 65 (1987) 541.

18 Tao W Q, *J Heat Transf ASME Trans*, 109 (1987) 791.
19 Oliveira L S, Haghighi K, *Numer Heat Trans A*, 34 (1998) 105.
20 Lamnatou C, Papanicolau E, Belessiotis V & Kyriakis N, *Numer Heat Trans*, 56 (2009) 379.
21 Kaya A, Aydın O & Dincer I, *Int J Heat Mass Trans*, 49 (2006) 3094.
22 Mohan Chandra V P & Talukdar P, *Int J Heat Mass Trans*, 53 (2010) 4638.
23 De Bonis M V & Ruocco G, *J Food Eng*, 89 (2008) 232.
24 Suresh H N, Aswatha Narayana P A & Seetharamu K N, *Heat Mass Trans*, 37 (2001) 205.
25 Badruddin I A, Zainal Z A, Narayana P A, Seetharamu K N & Siew L W, *Int J Therm Sci*, 45 (2006) 487.
26 Badruddin I A, Zainal Z A, Narayana P A, Seetharamu K N & Siew L W, *Int J Numer Meth Eng*, 65 (2006) 2265.
27 Badruddin I A, Zainal Z A, Narayana P A & Seetharamu K N, *Int Commun Heat Mass Trans*, 33(4) (2006). 491.
28 Nik-Ghazali N, Badrudin I A, Badruddin A & Tabatabaeikia S, *Adv Mech Eng*, 6 (2014) 209753.
29 Walker K L & Homsy G M, *J Fluid Mech*, 87 (1978) 449.
30 Bejan A, *Lett Heat Mass Trans*, 6 (1979) 93.
31 Gross R J, Bear M R, Hickox C E, *The application of flux-corrected transport (FCT) to high Rayleigh number natural convection in a porous medium*, in: *Proceedings of 8th Int. Heat Transfer Conf*, San Francisco, CA, USA (1986).
32 Manole D M & Lage J L, *Heat Mass Trans Porous Med, ASME Conference*, 55 (1992) 216.
33 Bekermann C, Viskanta R & Ramadhyani S, *Numer Heat Trans Part A*, 10 (1986) 557.
34 Moya S L, Ramos E & Sen M, *Int J Heat Mass Trans*, 30 (1987) 741.
35 Baytas A C & Pop I, *Int J Heat Mass Trans*, 42 (1999) 1047.
36 Misirlioglu A, Baytas A C & Pop I, *Int J Heat Mass Trans*, 48 (2005) 1840.